Photovoltaic properties of low-bandgap (0.7–0.9 eV) lattice-matched GaInNAsSb solar junctions grown by molecular beam epitaxy on GaAs

Riku Isoaho[a], Arto Aho[a], Antti Tukiainen[a], Timo Aho[a], Marianna Raappana[a], Turkka Salminen[b], Jarno Reuna[a], and Mircea Guina[a]

[a] Optoelectronics Research Center, Physics Unit, Tampere University, P.O. Box 692, FI-33101, Tampere, Finland

[b] Microscopy Center, Tampere University, P.O. Box 692, FI-33101, Tampere, Finland

Abstract

We demonstrate single junction GaInNAsSb solar cells with high nitrogen content, i.e. in the range of 5 to 8%, and bandgap energies close to 0.7 eV grown by molecular beam epitaxy. A good crystalline quality is demonstrated for the entire range of N concentrations. An average external quantum efficiency of 0.45 is demonstrated for GaInNAsSb solar cell with 6.2% N exhibiting a bandgap of 0.78 eV (no antireflection coatings has been applied). The internal quantum efficiency for the cell is 0.65 at E_g + 0.2 eV. The solar cells exhibited bandgap-voltage offsets between 0.55 V (for N = 5.3%) and 0.66 V (for N = 7.9%). When used in a six-junction solar cell architecture under AM1.5D illumination, the estimated short-circuit current density corresponding to the 0.78 eV cell is 8.2 mA/cm^2. Furthermore, using the parameters obtained for the GaInNAsSb junction with 6.2% N, we have estimated that such six-junction solar cell architecture could realistically attain an efficiency of over 50% at 1000 suns concentration.

Keywords: dilute nitrides, molecular beam epitaxy, GaInNAsSb, multijunction solar cells

1. Introduction

Multijunction solar cells (MJSC) based on III–V materials demonstrate the highest conversion efficiencies of any photovoltaic devices. Currently, the highest efficiency of 46% has been achieved with a wafer-bonded III–V based four-junction (4J) device under concentrated illumination [1]. Conversion efficiencies exceeding 50% could theoretically be demonstrated with a 4J architecture [2,3] and by further increasing the number of junctions, efficiencies over 60% have been predicted [3,4]. To this end, development of new sub-junction materials, preferably lattice-matched to GaAs or Ge, is needed.

The most commonly used MJSCs are based on lattice-matched GaInP/GaInAs/Ge triple-junction cells [5]. However, the bandgap energy (E_g) of the Ge bottom junction is 0.67 eV, which is often not optimal for cell designs with a higher number of junctions [6]. For example, lattice-matched MJSCs with six junctions would need a lattice-matched junction material with E_g in the range of 0.8 eV to 0.7 eV. These conditions can be met by dilute nitride materials, i.e. GaInNAsSb; by incorporating only a few atomic percent of N it is in principle possible to reach bandgaps ranging from 1.4 eV down to 0.7 eV [7]. Historically, these materials have suffered from short minority carrier lifetimes [8] and high background doping levels [9], yet dilute nitrides with approximately 3% N (corresponding to bandgaps around 1 eV) grown by molecular beam epitaxy (MBE) have successfully been utilized in high-efficiency MJSCs [7,10,11]. In addition, dilute nitrides with bandgaps around 0.8 eV have already been demonstrated [7,12,13] but the photovoltaic properties of these materials have been generally modest.

In this work, we report on the development of lattice-matched GaInNAsSb materials with high nitrogen content (i.e. 6% to 8%) and report on performance of single junction GaInNAsSb solar cells with bandgaps down to ~0.7 eV. The material compositions are determined by energy-dispersive spectroscopy (EDS), while x-ray diffraction (XRD) is used to assess the crystallographic quality. The photovoltaic properties of the structures are investigated by current-voltage and quantum efficiency measurements. Finally, using realistic parametrization, we estimate the performance potential of a six-junction (6J) solar cell design incorporating the narrow bandgap GaInNAsSb material as the bottom junction.

2. Experimental

A set of single-junction GaInNAsSb p-i-n solar cells with varying material compositions was fabricated using a Veeco GEN20 plasma-assisted solid source MBE system equipped with SUMO cells for group III elements and valved cracker sources for As, P and Sb. A radio frequency plasma source was used for generation of atomic N. The structures were grown on 3" n-GaAs(100) substrates and consisted of a GaInNAsSb layer with a thickness of 700 nm, which was sandwiched between p-GaAs and n-GaAs layers with a thickness of 100 nm each. A GaInP back surface field layer with a thickness of 100 nm was used on the p-side, and a 40 nm thick GaInP window layer was used on the n-side. The In composition of the GaInNAsSb layers was nominally 15% for all the structures. The bandgap of the GaInNAsSb material was varied by changing the nominal N composition in the range of 5.2–8.3%. The nominal N compositions were estimated by using an incorporation model described in [14]. Other growth parameters for the GaInNAsSb layers were kept constant for all the samples; the chosen growth conditions were based on growth parameter optimization made for ~1 eV GaInNAs and GaInNAsSb materials [15,16]. The nominal N compositions of the samples and corresponding naming are given in Table 1.

Table 1. Nominal nitrogen compositions for the GaInNAsSb p-i-n structures.

Sample	S1	S2	S3	S4
Nominal [N] (%)	5.2	5.8	6.0	8.3

The optical quality of the materials was characterized by room temperature photoluminescence (PL) measured with an Accent RPM2000 PL mapper using 980 nm laser excitation. The crystal quality and lattice-matching of the materials was assessed with high-resolution x-ray diffraction (XRD) by measuring ω-2θ scans around the (004) reflections using a Philips X'Pert Pro triple-axis XRD system. Additional XRD characterization for selected structures was performed by measuring reciprocal space maps (RSM) around symmetric (004) and asymmetric (-2-24) reflections using a Panalytical X'pert^3 XRD system equipped with a PIXcel3D detector. For the (-2-24) RSMs, a grazing exit configuration was used. The compositions of the GaInNAsSb layers were investigated by EDS measurements on the facets of the GaInNAsSb layers; we used a Zeiss Crossbeam 540 scanning electron microscope (SEM) with an Oxford Instruments X-Max 80 silicon-drift detector and an acceleration voltage of 5 kV.

The wafers were processed into 6 mm × 6 mm solar cells with an active area of 0.25 cm^2. No antireflection coatings (ARC) were deposited. The electrical performance of the cells was investigated by measuring dark current-voltage (dark-IV), light-biased current-voltage (light-IV), and external quantum efficiency (EQE). The IV characteristics were measured at 25°C using an OAI TriSol 7 kW CPV-simulator, with ASTM G173-03 AM1.5D (1000 W/m^2 normalization) as the reference spectrum for the light-IV measurements. Additional light-IV measurements under concentration were conducted for S3 with concentration factors between 0.5 and 2.6. The EQE measurements were performed with an in-

house built monochromator based EQE setup equipped with an Oriel 250 W QTH lamp. The EQE system was calibrated with reference Ge and Si detectors.

3. Results and discussion

The room temperature PL spectra for as-grown GaInNAsSb samples are presented in Fig. 1. The PL peak of the sample S4 could not be resolved with the InGaAs detector (Hamamatsu C7251) as the response of the detector is limited to 1700 nm [17]. When the peak emission wavelength shifts towards longer wavelengths corresponding to increasing N concentrations, the PL properties of the materials degrade rapidly; the PL intensity is reduced approximately tenfold for S3 (peak at 1560 nm) compared to S1 (peak at 1445 nm). The direct comparison of the PL intensities is justified as the response of the InGaAs detector is close to constant in this wavelength range [17]. In addition, Fig. 1 reveals that the full width at half-maximum (FWHM) of the PL peak increases from 57 meV (S1) to 76 meV (S3). For comparison, our highest quality 1 eV GaInNAsSb materials exhibit a FWHM of ~30 meV. The significant increase in the FWHM with increasing N content could be associated with a higher density of localized electronic states in the bandgap due to incorporation of N.

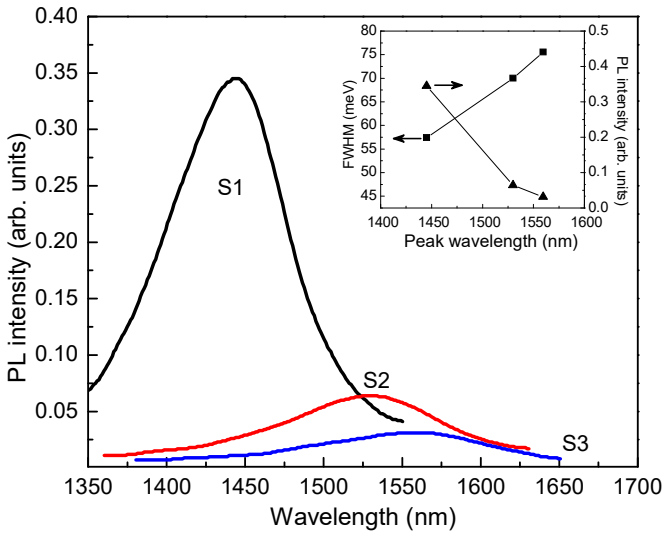

Figure 1. Room temperature PL spectra measured for S1, S2 and S3 with 980 nm excitation. The inset shows the evolution of PL peak full width at half-maximum (FWHM) and PL intensity as with respect to PL peak wavelength.

The XRD rocking curves measured from the (004) planes revealed that the GaInNAsSb layers for S1, S2 and S3 were compressively strained with S3 being closest to being fully lattice-matched. The lattice mismatches for S1, S2 and S3 were 0.249%, 0.102% and 0.006%, respectively. Only S4 exhibited tensile strain with lattice mismatch of -0.389%. The large lattice mismatch in S4 indicates incorporation of a substantial amount of N into the crystal, as was already expected from the nominal N composition of 8.3%.

RSMs measured around (004) and (-2-24) reflections for S3 and S4 were used to reveal possible relaxation or tilting in the crystals and to assess the crystalline quality. The RSMs obtained for S4 are illustrated in Fig. 2, which shows that the GaInNAsSb peak in S4 is not broadened compared to the substrate peak, indicating good crystalline quality even with high N concentrations. In addition, the epilayer peak in the asymmetric (-2-24) scan is aligned on the same vertical line with the substrate peak indicating excellent lattice coherence with the substrate. Similar observations were made also for S3. Peak analysis of the RSMs with X'Pert Epitaxy software indicated strain relaxation of 0.0% ± 0.1% for the GaInNAsSb layers in S3 and S4.

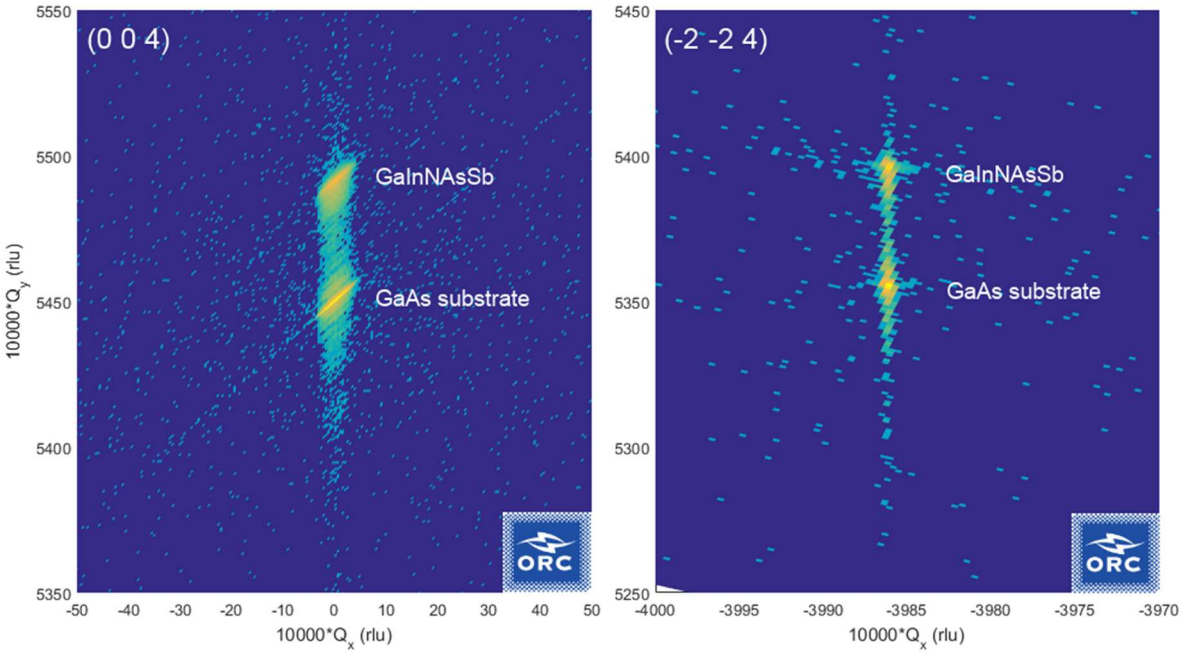

Figure 2. RSMs for sample S4 around (004) and (-2-24) reflections.

EDS measurements were employed to determine directly the In, Sb and N compositions for the GaInNAsSb materials. Due to the low atomic number of nitrogen, accurate and reliable detection of dilute concentrations of N has typically been difficult by EDS, which is why compositions determined solely by EDS for dilute nitride III–Vs are not widely reported. However, recent developments in the EDS analysis of light elements has enabled more accurate detection of N [18]. The material compositions revealed by EDS are shown in Table 2.

Table 2. GaInNAsSb compositions determined from EDS measurements.

Sample	[In] (%)	[N] (%)	[Sb] (%)	$[N]_{EDS}/[N]_{nominal}$
S1	16	5.3	1.4	1.02
S2	16	6.0	1.8	1.03
S3	16	6.2	1.4	1.03
S4	16	7.9	0.9	0.95

The In and N compositions measured by EDS are well in line with the targeted composition values shown in Table 1. The nitrogen compositions determined by EDS are within ± 5% from the nominal values for all the samples, which shows that the N concentration can be reliably determined by EDS. Moreover, this also proves the applicability of the plasma model we proposed in [14] for estimating the N compositions. In practice, this means that the incorporation probability from the N atom flux does not change, even though the N composition is as large as 8%. The bandgaps and lattice constants for the materials were evaluated from the EDS data by using the equations and the modified band anti-crossing (BAC) model described in Ref [19]. The calculated lattice constants agree with the values determined from the XRD measurements as the relative errors between the calculated and measured lattice parameters are within ± 0.1%. The error arises mostly from the uncertainty of composition determination by EDS, which is ± 1 percentage points. The bandgap energies calculated with the BAC-model are slightly larger (40-80 meV) than the measured E_g values (Table 3). The difference between the calculated and measured bandgaps is assumed to mainly arise from the unknown short range ordering state of the crystal and the inaccuracy of the BAC-model with relatively high In and N concentrations, which can also be seen in Ref. [19] describing the model. The EDS data also shows that

the measured Sb concentration peaks for ~6% N beyond which the concentration of Sb starts to decrease. This might indicate competition between N and Sb atoms for the same lattice sites.

The bandgap energies of the GaInNAsSb materials were estimated from the derivatives of the EQE curves [20], which yielded E_g values between 0.73 eV and 0.86 eV. The lowest E_g of 0.73 eV, measured for S4 is only approximately 40 meV larger than the bandgap of Ge. The measured EQE curves are illustrated in Fig. 3. From here one can clearly see that S3 (E_g = 0.78 eV) exhibits the best EQE within the sample set, which is rather surprising when considering the measured N concentration of 6.2%. The EQE performance of S3 in the range of 1400-1600 nm is 3 to 5 times higher than what has been reported for a 0.77 eV dilute nitride cells in Ref. [13]. In addition, the EQE performance of S4 (E_g = 0.73 eV) is better than for the best dilute nitride cell with E_g = 0.77 eV reported earlier [13].

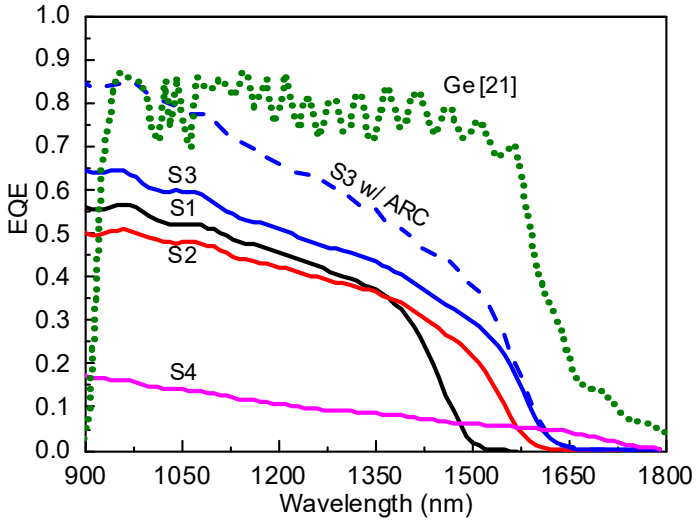

Figure 3. EQE spectra measured for the GaInNAsSb p-i-n structures without ARC (solid lines) and estimated EQE for S3 with 4-layer TiO_2/SiO_2 ARC (dashed line). For comparison, EQE of a Ge-junction extracted from Ref. [21] (dotted line) is shown.

The short-circuit current densities (J_{sc}) of the solar cell samples were estimated from the EQE spectra by integrating the product of the EQE and the photon flux density of the ASTM G173-03 AM1.5D (1000 W/m^2 normalization) spectrum at wavelengths above 900 nm. The calculated J_{sc} values were compared to ideal J_{sc} values calculated with unity EQEs. The wavelength range above 900 nm was chosen for the J_{sc} calculations because these materials are intended to be used as a bottom cell in a multijunction solar cell (for replacing the Ge junction), thus limiting the part of the spectrum that can be used by these subcells into this wavelength range. This number is also directly comparable with the J_{sc} of Ge subjunction within GaInP/Ga(In)As/Ge architecture. The average external quantum efficiency (EQE_{ave}) was estimated by taking the ratio between the calculated and ideal J_{sc} values. The significant material and performance parameters extracted from the EQE data are compiled in Table 3.

Table 3. Parameters extracted from the EQE results for the GaInNAsSb solar cells. The J_{sc} values were calculated at wavelengths above 900 nm using ASTM G173-03 AM1.5D (1000 W/m^2 normalization) as the reference spectrum. Ideal J_{sc} values represent the highest obtainable current densities with unity EQE at above 900 nm wavelengths. For comparison, corresponding values calculated for a Ge-junction from Ref. [21] are also presented.

Sample	E_g (eV)	Calculated J_{sc} (mA/cm^2)	Ideal J_{sc} (mA/cm^2)	EQE_{ave}
S1	0.85	9.9	22.0	0.45
S2	0.80	9.3	24.9	0.37
S3	0.78	11.8	26.5	0.45
S4	0.73	2.9	28.9	0.10

Ge [21]	0.67	18.6	29.1	0.64

The internal quantum efficiencies (IQE) of the cells were calculated from the EQE data assuming optically thick junction by dividing the measured EQEs by factor 1-*R*, where *R* is the measured surface reflectance. Table 4 shows IQE values taken at E_g + 0.2 eV for comparison with the literature values.

Table 4. IQE values at E_g + 0.2 eV calculated from the EQE data.

Sample	E_g (eV)	IQE at E_g + 0.2 eV	Reference
S1	0.85	0.63	This work
S2	0.80	0.56	This work
S3	0.78	0.65	This work
S4	0.73	0.12	This work
GaInNAs	0.90	0.24	[13]
GaInNAsSb	0.77	0.16	[13]
GaInNAsSb	0.92	0.72	[9]

The IQE at E_g + 0.2 eV for the best cell (S3) shows an increase by at least four-fold compared to the GaInNAsSb cell with similar E_g (0.77 eV) reported in Ref. [13]. Even though the E_g for S4 is 40 meV smaller than for GaInNAsSb in Ref. [13], the IQE at E_g + 0.2 eV is only 4 percentage points lower for S4. In addition, the IQE data for S3 was used to estimate the EQE for the S3 with a simulated 4-layer TiO_2/SiO_2 antireflection coating (ARC), which is shown in Fig. 3.

The calculated IQE of S3 was used to estimate the J_{sc} of such subcell in a multijunction configuration, where the light entering the subcell would be filtered by another subcell on top of the analyzed junction. The J_{sc} values were calculated by assuming optically thick filtering subcells with different bandgap energies as well as different ARCs. The calculations were made by using AM1.5 (1000 W/m^2) spectrum. The projected J_{sc} values for S3 in multijunction configuration are presented in Fig. 4. With a thick 1.0 eV subcell on top of S3, the bottom junction is expected to generate 2.9 mA/cm^2 at AM1.5D (1000 W/m^2) without ARC. With a 4-layer TiO_2/SiO_2 ARC the J_{sc} is projected to increase to 3.8 mA/cm^2. In a more ideal scenario, a subcell with the same E_g as S3 but with an average EQE of 0.95, the J_{sc} is estimated to be 7.9 mA/cm^2. A more realistic target that could be reached with further optimization of the materials and advanced cell processing, would be an average EQE of 0.90 at photon energies below 1 eV corresponding to J_{sc} of 7.4 mA/cm^2.

The electrical properties of the solar cells were characterized by light-IV and dark-IV measurements. From the light-IV data values for J_{sc}, open-circuit voltage (V_{oc}) and fill factor (*FF*) were extracted. The dark-IV measurements were used to estimate the dark current densities (J_0). In addition, the bandgap-voltage offsets ($W_{oc} = E_g/q - V_{oc}$) were calculated from the bandgap values determined from the EQE data and the measured V_{oc} values. The light-IV curves are shown in Fig. 5 and the IV characteristics are summarized in Table 5.

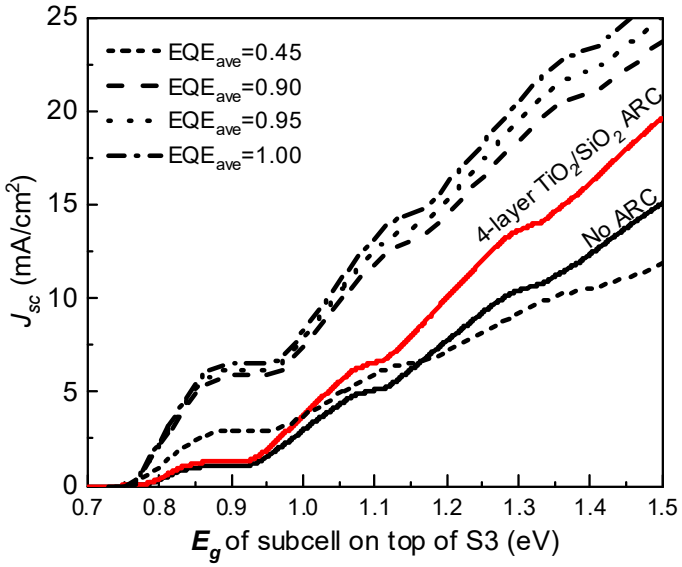

Figure 4. Estimated J_{sc} for S3 if employed in a multijunction configuration with varying optically thick filtering subcell under AM1.5D (1000 W/m^2) illumination. The short dashed, dashed, dotted and dash-dotted lines represent the upper limits for J_{SC} of a 0.78 eV subcell with average EQEs of 0.45, 0.90, 0.95 and 1.00, respectively.

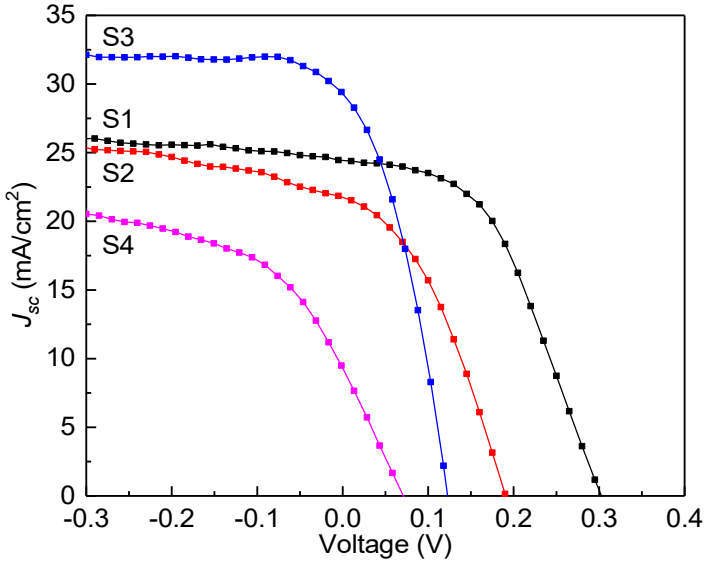

Figure 5. Measured light-IV curves for the GaInNAsSb p-i-n structures without ARC under full spectrum AM1.5D (1000 W/m^2) illumination.

Table 5. IV characteristics for the p-i-n cells at full spectrum AM1.5D (1000 W/m^2) excitation.

Sample	J_{sc} (mA/cm^2)	V_{oc} (V)	W_{oc} (V)	FF	J_0 (A/cm^2)
S1	24.5	0.30	0.55	0.47	3.9e-6
S2	21.7	0.19	0.61	0.38	5.0e-4
S3	29.2	0.12	0.66	0.37	2.1e-3
S4	9.3	0.07	0.66	0.25	2.6e-3

As expected, the V_{oc} values decrease with lower bandgaps (see Fig. 6), but at the same time W_{oc} increases. For S1 with E_g=0.85 eV the W_{oc} is 0.55 V, which is a typical value for dilute nitride SCs [22,23]. For 0.8 eV bandgap the W_{oc} already exhibits significant increase, and with bandgaps below 0.8 eV the V_{oc} values start to follow $V_{oc} = E_g/q–0.66\ V$ dependence, indicating decrease in material quality. For high quality GaAs cells bandgap-voltage offsets of 0.4 V is expected [24], and W_{oc} of 0.49 V has been demonstrated for a 1 eV dilute nitride cell [25].

The *FF*s decrease almost linearly with the bandgap of the GaInNAsSb layer. The major contribution to the degradation of *FF* is thought to arise from the increased J_0 with respect to lower E_g (Table 4). For S1 the J_0 value is of the same magnitude as reported for other dilute nitride cells with ~1 eV bandgaps [13,26]. For S3 and S4, with bandgaps below 0.8 eV, three orders of magnitude higher J_0 values are determined when compared to S1. Nevertheless, the J_0 values for S3 and S4 are approximately 50% smaller than J_0 reported for 0.77 eV cell in Ref. [13]. In addition, the light-IV measurements for S3 performed with soft concentrations revealed a logarithmic dependence between the cell V_{oc} and concentration factor. The fitted expression for V_{oc} as function of concentration was used to estimate the ideality factor (n) for S3, yielding n = 1.57, which is closely comparable to ideality factors reported for 1 eV GaInNAs cells [26,27].

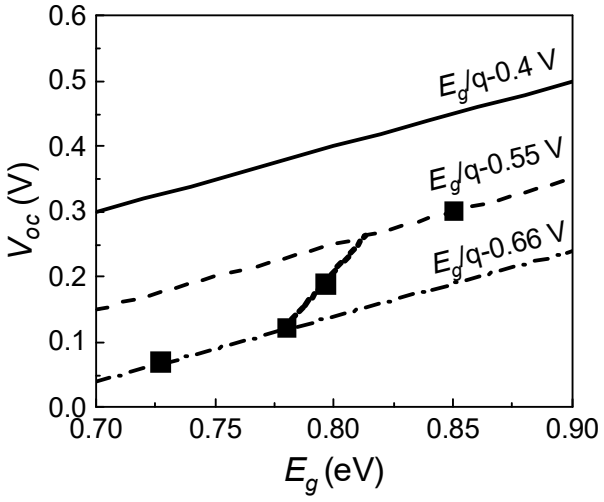

Figure 6. V_{oc} values measured with AM1.5D (1000 W/m^2) for the GaInNAsSb cells (black squares) as a function of measured E_g of GaInNAsSb. The dashed and dash-dotted lines show the upper and lower limits of bandgap-voltage offset measured for the sample set. The solid black line represents bandgap-voltage offset of 0.4 V commonly measured for high quality GaAs cells.

The efficiency potential for a 6J design employing dilute nitride material with 6% N and 0.78 eV bandgap for the bottom junction was estimated by diode modelling using realistic subcell parameters. For all the other subcells except for the 0.78 eV GaInNAsSb subcell, an ideality factor of 1.5 was assumed. Based on the IV results an ideality factor of 1.57 was used for the bottom junction. For subcells 1-4, a bandgap-voltage offset of 0.4 V was used. For subcell 5 we used a bandgap-voltage offset value of 0.5 V. Based on the IV results, W_{oc} of 0.66 V was used for the bottom junction. The W_{oc} values were determined using the data of one-sun IV measurements. More detailed discussion about the model parameters and validation of the model can be found elsewhere [28]. In addition, the efficiency potential for a 6J design employing improved 0.78 eV GaInNAsSb material was estimated. For the calculations, it was assumed that series resistance is similar to 1 eV dilute nitride materials, and that the junction above the bottom junction is sufficiently thin to pass a fraction of the light into the bottom junction. The 6J efficiencies were estimated by employing different top cells with bandgap

energies between 2.0 eV and 2.2 eV. With the current material quality the bandgaps for the subcells 2–5 were 1.92 eV, 1.63 eV, 1.40 eV and 1.18 eV, respectively.

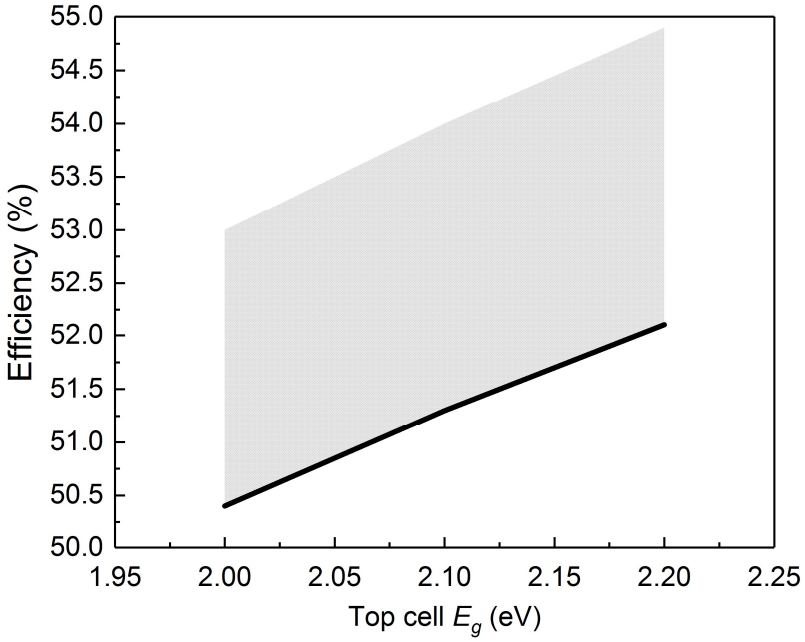

Figure 7. Projected conversion efficiencies (black line) for optimized 6J cell designs employing the current 0.78 eV GaInNAsSb material as the bottom junction and varying top cell bandgaps at 1000 suns. The shaded region illustrates estimated efficiency potential of a 6J cell with improvements for the 0.78 eV material.

By employing the 0.78 eV GaInNAsSb material for the bottom cell, the J_{sc} of the 6J is estimated to be 8.2 mA/cm^2. With a 2.0 eV top cell, the efficiency of the 6J is projected to reach 50.4% at 1000 suns. By replacing the 2.0 eV top cell with a 2.2 eV junction, the 6J efficiency would increase to 52.1%.

4. Conclusions

We have demonstrated MBE-grown single junction GaInNAsSb cells with up to ~8% N concentrations and bandgap energies close to 0.7 eV. Although the N content is very high, the materials exhibited good crystalline quality and morphology. The compositions of the GaInNAsSb layers were estimated by direct EDS measurements, yielding compositions close to the target values. The SC with 6.2% N exhibited the best performance; the average EQE for the SC without ARC and the IQE at E_g + 0.2 eV were estimated to be 0.45 and 0.65, respectively. The light-IV characterization at AM1.5D (1000 W/m^2) showed that the SC with 6.2% N generated a J_{sc} of 29.2 mA/cm^2. The bandgap-voltage offsets for the SCs were determined to between 0.55 and 0.66, which are comparable to values reported typically for dilute nitrides. In addition, the dark-IV measurements revealed that J_0 increases rapidly with higher N contents. We also employed diode modelling to project efficiency for 6J design employing these GaInNAsSb materials, and concluded that with the current material quality it is already possible to achieve efficiencies above 50%.

Acknowledgements

The financial support provided by the European Research Council (ERC AdG AMETIST, #695116) is acknowledged. The authors also acknowledge MSc Lauri Hytönen for his technical support.

References

[1] M.A. Green, Y. Hishikawa, E.D. Dunlop, D.H. Levi, J. Hohl-Ebinger, A.W.Y. Ho-Baillie, Solar cell efficiency tables (version 51), Prog Photovoltaics Res Appl. 26 (2018) 3-12.

[2] D.J. Friedman, Progress and challenges for next-generation high-efficiency multijunction solar cells, Current Opinion in Solid State and Materials Science. 14 (2010) 131-138.

[3] C.H. Henry, Limiting efficiencies of ideal single and multiple energy gap terrestrial solar cells, J. Appl. Phys. 51 (1980) 4494-4500.

[4] M. Yamaguchi, K. Nishimura, T. Sasaki, H. Suzuki, K. Arafune, N. Kojima, Y. Ohsita, Y. Okada, A. Yamamoto, T. Takamoto, K. Araki, Novel materials for high-efficiency III–V multi-junction solar cells, Solar Energy. 82 (2008) 173-180.

[5] P. T. Chiu, D. C. Law, R. L. Woo, S. B. Singer, D. Bhusari, W. D. Hong, A. Zakaria, J. Boisvert, S. Mesropian, R. R. King, N. H. Karam, Direct Semiconductor Bonded 5J Cell for Space and Terrestrial Applications, IEEE Journal of Photovoltaics. 4 (2014) 493-497.

[6] L. Zhu, T. Mochizuki, M. Yoshita, S. Chen, C. Kim, H. Akiyama, Y. Kanemitsu, Conversion efficiency limits and bandgap designs for multi-junction solar cells with internal radiative efficiencies below unity, Opt Express. 24 (2016) 740-751.

[7] V. Sabnis, H. Yuen, M. Wiemer, High-efficiency multijunction solar cells employing dilute nitrides, AIP Conference Proceedings. 1477 (2012) 14-19.

[8] D. J. Friedman, A. J. Ptak, S. R. Kurtz, J. F. Geisz, Analysis of depletion-region collection in GaInNAs solar cells, Conference Record of the Thirty-first IEEE Photovoltaic Specialists Conference, 2005. (2005) 691-694.

[9] D.B. Jackrel, S.R. Bank, H.B. Yuen, M.A. Wistey, J.S. Harris, A.J. Ptak, S.W. Johnston, D.J. Friedman, S.R. Kurtz, Dilute nitride GaInNAs and GaInNAsSb solar cells by molecular beam epitaxy, J. Appl. Phys. 101 (2007) 114916.

[10] A. Aho, R. Isoaho, A. Tukiainen, V. Polojärvi, M. Raappana, T. Aho, M. Guina, Performace of Dilute Nitride Triple Junction Space Solar Cell Grown by MBE, E3S Web Conf. 16 (2017) 03008.

[11] A. Tukiainen, A. Aho, G. Gori, V. Polojärvi, M. Casale, E. Greco, R. Isoaho, T. Aho, M. Raappana, R. Campesato, M. Guina, High-efficiency GaInP/GaAs/GaInNAs solar cells grown by combined MBE-MOCVD technique, Prog Photovoltaics Res Appl. (2016) 914–919.

[12] F. Suarez, T. Liu, A. Sukiasyan, J. Lang, E. Pickett, E. Lucow, T. Bilir, S. Chary, R. Roucka, I. Aeby, L. Zhang, S. Siala, Advances in Dilute Nitride Multi-Junction Solar Cells for Space Power Applications, E3S Web Conf. 16 (2017) 03006.

[13] S.L. Tan, W.M. Soong, M.J. Steer, S. Zhang, J.S. Ng, J.P.R. David, Dilute nitride GaInNAs and GaInNAsSb for solar cell applications, Proc. SPIE 8256, Physics, Simulation, and Photonic Engineering of Photovoltaic Devices. 8256 (2012) 82561E.

[14] A. Aho, V.-. Korpijärvi, A. Tukiainen, J. Puustinen, M. Guina, Incorporation model of N into GaInNAs alloys grown by radio-frequency plasma-assisted molecular beam epitaxy, J. Appl. Phys. 116 (2014).

[15] A. Aho, A. Tukiainen, V. Korpijärvi, V. Polojärvi, J. Salmi, M. Guina, Comparison of GaInNAs and GaInNAsSb solar cells grown by plasma-assisted molecular beam epitaxy, AIP Conference Proceedings. 1477 (2012) 49-52.

[16] A. Aho, V. Polojärvi, V. Korpijärvi, J. Salmi, A. Tukiainen, P. Laukkanen, M. Guina, Composition dependent growth dynamics in molecular beam epitaxy of GaInNAs solar cells, Solar Energy Mater. Solar Cells. 124 (2014) 150-158.

[17] Hamamatsu Photonics, InGaAs multichannel detector head C7221, C7251, C7369, (2001).

[18] D.E. Newbury, N.W.M. Ritchie, Performing elemental microanalysis with high accuracy and high precision by scanning electron microscopy/silicon drift detector energy-dispersive X-ray spectrometry (SEM/SDD-EDS), J. Mater. Sci. 50 (2015) 493-518.

[19] A. Aho, V. Korpijärvi, R. Isoaho, P. Malinen, A. Tukiainen, M. Honkanen, M. Guina, Determination of composition and energy gaps of GaInNAsSb layers grown by MBE, J. Cryst. Growth. 438 (2016) 49-54.

[20] D. Aiken, M. Stan, C. Murray, P. Sharps, J. Hills, B. Clevenger, Temperature dependent spectral response measurements for III-V multi-junction solar cells, Conference Record of the Twenty-Ninth IEEE Photovoltaic Specialists Conference, 2002. (2002) 828-831.

[21] G. Siefer, C. Baur, A. W. Bett, External quantum efficiency measurements of Germanium bottom subcells: Measurement artifacts and correction procedures, 2010 35th IEEE Photovoltaic Specialists Conference. (2010) 000704-000707.

[22] N. Leong, K.H. Tan, W.K. Loke, S. Wicaksono, D. Li, S.F. Yoon, P. Sharma, T. Milakovich, M. Bulsara, G. Fitzgerald, Growth of 1-eV GaNAsSb-based photovoltaic cell on silicon substrate at different As/Ga beam equivalent pressure ratios, Progress in Photovoltaics: Research and Applications. 24 (2016) 340-347.

[23] A. Aho, A. Tukiainen, V. Polojärvi, J. Salmi, M. Guina, High current generation in dilute nitride solar cells grown by molecular beam epitaxy, Proc. SPIE 8620, Physics, Simulation, and Photonic Engineering of Photovoltaic Devices II. (2013) 86201I.

[24] R.R. King, D. Bhusari, A. Boca, D. Larrabee, X.- Liu, W. Hong, C.M. Fetzer, D.C. Law, N.H. Karam, Band gap-voltage offset and energy production in next-generation multijunction solar cells, Prog. Photovolt: Res. Appl. 19 (2010) 797-812.

[25] J. Tommila, A. Aho, A. Tukiainen, V. Polojärvi, J. Salmi, T. Niemi, M. Guina, Moth-eye antireflection coating fabricated by nanoimprint lithography on 1 eV dilute nitride solar cell, Prog Photovoltaics Res Appl. 21 (2013) 1158-1162.

[26] A. Aho, A. Tukiainen, V. Polojärvi, M. Guina, Performance assessment of multijunction solar cells incorporating GaInNAsSb, Nanoscale Research Letters. 9 (2014) 1-7.

[27] D. Jackrel, A. Ptak, S. Bank, H. Yuen, M. Wistey, D. Friedman, S. Kurtz, J.S. Harris, GaInNAsSb Solar Cells Grown by Molecular Beam Epitaxy, 2006 IEEE 4th World Conference on Photovoltaic Energy Conference. 1 (2006) 783-786.

[28] A. Aho, R. Isoaho, L. Hytönen, T. Aho, M. Raappana, V. Polojärvi, A. Tukiainen, J. Reuna, S. Mäkelä, M. Guina, Lattice-matched four-junction tandem solar cell including two dilute nitride bottom junctions, Prog Photovolt Res Appl. (2018).